Grant-Free Random Access in Multicell Massive MIMO Systems with Mixed-Type Devices: Backoff Mechanism Optimizations under Delay Constraints

Yingying Fang, and Qi Zhang*
Nanjing University of Posts and Telecommunications, Nanjing 210003, China
[e-mail: fangyingying0729@163.com; zhangqi1212@njupt.edu.cn]
*Corresponding author: Qi Zhang

Received April 24, 2022; revised August 6, 2022; revised November 29, 2022; accepted January 7, 2023; published January 31, 2023

Abstract

Grant-free random access (GFRA) can reduce the access delay and signaling cost, and satisfy the short transmission packet and strict delay constraints requirement in internet of things (IoT). IoT is a major trend in the future, which is characterized by the variety of applications and devices. However, most existing studies on GFRA only consider a single type of device and omit the effect of access delay. In this paper, we study GFRA in multicell massive multiple-input multiple-output (MIMO) systems where different types of devices with various configurations and requirements co-exist. By introducing the backoff mechanism, each device is randomly activated according to the backoff parameter, and active devices randomly select an orthogonal pilot sequence from a predefined pilot pool. An analytical approximation of the average spectral efficiency for each type of device is derived. Based on it, we obtain the optimal backoff parameter for each type of devices under their delay constraints. It is found that the optimal backoff parameters are closely related to the device number and delay constraint. In general, devices that have larger quantity should have more backoff time before they are allowed to access. However, as the delay constraint become stricter, the required backoff time reduces gradually, and the device with larger quantity may have less backoff time than that with smaller quantity when its delay constraint is extremely strict. When the pilot length is short, the effect of delay constraints mentioned above works more obviously.

Keywords: Backoff mechanism, delay constraints, GFRA, mixed-type devices, multicell massive MIMO.

1. Introduction

Machine-type communication (MTC) is one of the major tends for future wireless networks and the driving factor Internet of Things (IoT) [1]. Massive multiple-input multiple-output (MIMO), where each BS equipped with dozens or even hundreds of antennas serve tens of users, is regarded as a key support technology for MTC [2]. Massive MIMO can greatly increase the system capacity and has high robustness and low energy consumption [3,4]. It is also charactered by low cost and interference tolerance [5].

MTC has vast amount of devices that is larger than the available pilots. However, the conventional massive MIMO usually assumes a fully-loaded of devices, which is obviously not appropriate in MTC [6,7]. Therefore, we need to design an effective access scheme for devices in massive MIMO. The existing random access (RA) schemes of massive MIMO systems can be divided into two categories: grant-based and grant-free RA (GFRA) schemes [8-10]. In grant-based RA, the devices need to wait for the permission of the BS to transmit data, which will obviously increase the access delay [11]. In the GFRA scheme, the device directly transmits the pilot sequence and data to the BS without waiting for permission from the BS [12]. The detailed process of GFRA is given in the 3rd generation partnership project (3GPP) [13]. Obviously, compared with the grant-based RA scheme, GFRA scheme can reduce the transmission delay and signaling cost, which can satisfy the low lost and short delay requirement of MTC, and becomes popular in current research [14,15]. In [16], it proposes a GFRA scheme to reduce satellite access delay. In [17], it proposes a RA scheme of preamble-data superposition in massive MIMO system, which significantly improved access success rate and performance. These studies show that GFRA significantly improves the performance of massive MIMO system. Therefore, lots of works began to focus on the combination of massive MIMO and GFRA. The preamble code design scheme is proposed to achieve high success rate of device detection and channel estimation in massive MIMO GFRA system in [18]. In [19], it confirms the existence of an optimal pilot length that maximizes spectral efficiency in GFRA of massive MIMO systems. In [20], it analyzes the parameters that affect system capacity in massive MIMO GFRA system, such as the pilot length. However, all of the above studies considered single-cell scenarios. In [21], GFRA in multicell massive MIMO is studied. The backoff mechanism is usually applied on RA in 3GPP [22]. As the backoff parameter can be adjusted flexibly, some works focus on obtaining the optimal backoff parameter for GFRA [23, 24]. However, these works regard devices that select the same pilot as indistinguishable. In multicell systems, due to the large coverage of network, devices selecting the same pilot may located far away from each other, and the BS can detect the device under its coverage based on the distinction of received powers. Hence, a more precise analysis method is needed for the random access in multicell massive MIMO systems. Moreover, to enhance the device access success probability, we adopt the pilot reuse scheme which makes devices selecting the same pilot can be detected due to the low-level of interferences. Moreover, previous works on GFRA only consider one type of devices. In IoT, various kinds of applications result in different types of devices. Therefore, customized RA strategies should be provided for each type of devices according to their unique configurations and requirements. In addition, IoT devices usually have strict requirement on access delay. Therefore, we take the access delay into account, and set a delay constraint when optimizing the backoff parameter. This has also not been performed in existing literatures.

In this paper, we investigate GFRA in multicell massive MIMO systems with mixed-type devices with delay constraints. With backoff mechanism, each device is randomly activated, and the activated device randomly selects orthogonal pilot in the orthogonal pilot pool to send

frequently to the BS. We deduce the average spectral efficiency of each type of devices and the average spectral efficiency of all devices in each cell, and carry out simulation verification from all aspects. Based on it, we obtain the optimal backoff parameter for each type of devices under their delay constraints. It is found that the optimal backoff parameters are closely related to the devices number and delay constraints. In general, devices that have larger quantity should have more backoff time before they are allowed to access. However, as delay constraints become stricter, the required backoff time of devices reduces gradually, and the device with larger quantity may have less backoff time than that with smaller quantity when its delay constraint is extremely strict. Moreover, when the pilot length is short, the effect of delay constraints mentioned above works more obviously.

For ease of understanding, some of the symbols in this article are summarized in **Table 1**.

Table 1. Significance of symbols

Notation	Meaning
X^*	the conjugate of X
X^T	the transposition of X
X^H	the represents conjugate-transpose of X
U_{nkl}	the n -th device of the k -th type in the l -th cell
γ_{nkl}	the activation state of U_{nkl} , and $\gamma_{nkl} \in \{0,1\}$
$\delta_{nkl}^{(mk'i)}$	indicator shows whether U_{nkl} and $\mathsf{U}_{mk'i}$ choose the same pilot, and $\delta_{nkl}^{(mk'i)} \in \{0,1\}$
$\mathcal{C}_i$	co-pilot cells of the i -th cell
ρ_{nkl}	indicator shows whether U_{nkl} an intra-cell non-colliding device, and $\rho_{nkl} \in \{0,1\}$
$N_{\text{non},k}$	the average number of intra-cell non-colliding devices of the k -th type device per cell
$p_{\text{b},k}$	the backoff probability of the k -th type devices
$\mathcal{P}$	the average transmitted power of all devices
$\mathcal{D}_k$	the average delay for the k -th type of devices
$\mathcal{D}_k^{\text{u}}$	the delay constraint for the k -th type of devices

2. System Model

2.1 Channel Model

Consider a multicell MIMO wireless network with L cells as illustrated in **Fig. 1**, where each cell consists of a BS equipped with M antennas and N uniformly distributed devices with single antenna. There are K types of devices in the network, and the number of the k -th type of devices is N_k . That is, $\sum_{k=1}^{K} N_k = N$. The n -th device of the k -th type in the l -th cell is denoted as U_{nkl} . Devices transmit their data in the same time-frequency resource. The $M \times 1$ channel vector $\mathbf{g}_{inkl}$ between the i -th BS and U_{nkl} is given by

$$\mathbf{g}_{inkl} = \mathbf{h}_{inkl} \sqrt{\beta_{inkl}}, \tag{1}$$

where $\beta_{inkl} = q_{inkl} / d_{inkl}^{f}$ is the large-scale fading coefficient between the i -th BS and U_{nkl}

which models the path loss and shadow fading, while d_{inkl} is the distance between them, f is decay exponent, and q_{inkl} represents a log-normal random variable . $\mathbf{h}_{inkl} \sim \mathcal{CN}(0, \mathbf{I}_M)$ is the fast fading vector between the i-th BS and U_{nkl} .

2.2 Random Access

In RA, since the BS does not know which device requests access at this time slot, devices need to start the access by randomly selecting a pilot sequence and send it to the BS. In this process, different device may select the same pilot, which may result in the access fail. To improve the access success probability, we use the pilot reuse to extend the distance of devices selecting the same pilot, so that the pilot interference becomes negligible and the colliding devices from different cells can be detected.

We use the backoff mechanism to reduce the device conflict. The BS requires to calculate the device backoff parameters, and then broadcasts the backoff parameters to devices. The device randomly generates a backoff time according to the received backoff parameters broadcast to postpone the activation. When RA starts, the active device randomly selects a pilot sequence from the orthogonal pilot pool and sends it to the BS. Each pilot sequence consists of τ symbols, and thus the total number of orthogonal pilot sequences is also τ . Assuming the pilot reuse factor is α , then the number of pilots in each cell is τ / α . **Fig. 1** shows the system model diagram with $\alpha = 3$, we call the cells that use the same set of pilots as co-pilot cells. For example, cells with the same color in **Fig. 1** are co-pilot cells. We assume that the channel coherence time is T symbols long, and $T > \tau$. In each channel coherence interval, the active device directly transmits the orthogonal pilot along with data to the BS.

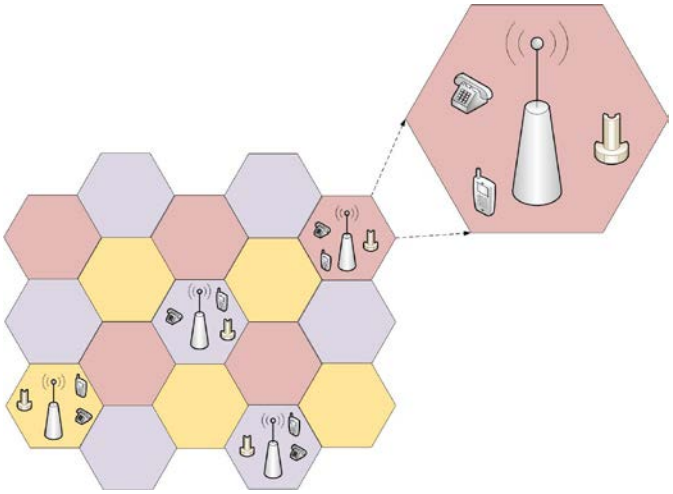

Fig. 1. Illustration of the multicell MIMO system with type of devices and pilot reuse factor $\alpha = 3$.

We call two devices who choose the same pilot as colliding devices. Colliding devices within the same cell cannot be distinguished by the BS. Hence, their access fail at this RA slot. However, if two colliding devices belong to different cells, even they select the same pilot, due to the pilot reuse, they locate far away from each other, and the BS can distinguish them based on the distinction on received power strength. Therefore, only devices does not conflict with other devices in the same cell can be successfully detected by the BS, and we call them as intra-cell non-colliding devices.

3. Performance Analysis

3.1 Channel Estimation

Due to the backoff mechanism, the k-th type of devices are randomly activated according to the backoff probability $p_{\mathrm{b},k}$. Let $\gamma_{nkl} \in \{0,1\}$, where $\gamma_{nkl} = 1$ denotes that U_{nkl} is active and $\gamma_{nkl} = 0$ that it is inactive. Let $\sqrt{\tau}\boldsymbol{\varphi}_{nkl} \in \mathbb{C}^{\tau \times 1}$ be the pilot sequence used by U_{nkl}. If U_{nkl} chooses the same pilot as $\mathsf{U}_{n'k'l'}$, we have $\boldsymbol{\varphi}_{nkl}^{H}\boldsymbol{\varphi}_{n'k'l'} = 1$. Otherwise, $\boldsymbol{\varphi}_{nkl}^{H}\boldsymbol{\varphi}_{n'k'l'} = 0$. Then, the $M \times \tau$ received matrix at the i-th BS can be written as

$$\mathbf{Y}_i = \sum_{l=1}^{L}\sum_{k=1}^{K}\sum_{n=1}^{N_k}\sqrt{\tau P_{nkl}}\mathbf{g}_{inkl}\boldsymbol{\varphi}_{nkl}^{T}\gamma_{nkl} + \mathbf{W}_i, \tag{2}$$

where P_{nkl} is the transmit power of U_{nkl}, and $\mathbf{W}_i$ is additive white Gaussian noise (AWGN) matrix, in which each element of $\mathbf{W}_i$ follows an independent distribution $\mathcal{CN}(0,1)$.

We assume that $\mathsf{U}_{mk'i}$ is the targeted device and does not collide with other devices in i-th cell. Then, the i-th BS estimates the channel of $\mathsf{U}_{mk'i}$ using $\mathbf{Y}_i\boldsymbol{\varphi}_{mk'i}^{*}$ as follows

$$\mathbf{Y}_i\boldsymbol{\varphi}_{mk'i}^{*} = \sqrt{\tau P_{mk'i}}\mathbf{g}_{mk'i} + \sum_{l\in\mathcal{C}_i}\sum_{k=1}^{K}\sum_{n=1}^{N_k}\sqrt{\tau P_{nkl}}\mathbf{g}_{inkl}\delta_{nkl}^{(mk'i)} + \boldsymbol{\omega}_i, \tag{3}$$

where $\mathcal{C}_i$ is the co-pilot cells of the i-th cell, and $\delta_{nkl}^{(mk'i)} \in \{0,1\}$ indicates whether $\mathsf{U}_{mk'i}$ select the same pilot as U_{nkl} ($\delta_{nkl}^{(mk'i)} = 1$) or not ($\delta_{nkl}^{(mk'i)} = 0$). Therefore, the estimates of $\mathbf{g}_{imk'i}$ can be written as

$$\hat{\mathbf{g}}_{imk'i} = \frac{1}{\sqrt{\tau P_{imk'i}}}\mathbf{Y}_i\boldsymbol{\varphi}_{mk'i}^{*} \tag{4}$$

Further, (4) can be represented as (5)

$$\hat{\mathbf{g}}_{imk'i} = \mathbf{g}_{imk'i} + \sum_{l\in\mathcal{C}_i}\sum_{k=1}^{K}\sum_{n=1}^{N_k}\sqrt{\frac{P_{nkl}}{P_{mk'i}}}\mathbf{g}_{inkl}\delta_{nkl}^{(mk'i)} + \frac{1}{\sqrt{\tau P_{imk'i}}}\boldsymbol{\omega}_i \tag{5}$$

From (5), we can see that the channel estimation of intra-cell non-colliding devices will be interfered not only by Gaussian white noise, but also by devices in the co-pilot cells. Using the estimated channels obtained above, we can then obtain the average spectral efficiency.

3.2 Average Spectral Efficiency

We can get that the received $M \times 1$ signal at the i-th BS is given by (6), where x_{nkl} is the data symbol with $\mathbb{E}\{|x_{nkl}|^2\} = 1$, and $\mathbf{o}_i$ is AWGN vector, and $\mathbf{o}_i \sim \mathcal{CN}(0,\mathbf{I}_M)$. Note that $\mathbf{r}_i$ is divided into five independent terms. The first term is the effective signal. The second and third terms indicate interference from other devices in the same cell. The fourth term represents interference from devices in other cells. The fifth term is noise.

$$\begin{aligned}\mathbf{r}_i &= \sqrt{P_{mk'i}}\mathbf{g}_{imk'i}x_{mk'i} + \sum_{n=1,n\neq m}^{N_k}\sqrt{P_{nk'i}}\mathbf{g}_{ink'i}x_{nk'i}\gamma_{nk'i} \\ &+ \sum_{k=1,k\neq k'}^{K}\sum_{n=1}^{N_k}\sqrt{P_{nki}}\mathbf{g}_{inki}x_{nki}\gamma_{nki} + \sum_{l=1,l\neq i}^{L}\sum_{k=1}^{K}\sum_{n=1}^{N_k}\sqrt{P_{nkl}}\mathbf{g}_{inkl}x_{nkl}\gamma_{nkl} + \mathbf{o}_i.\end{aligned} \tag{6}$$

Since $\mathsf{U}_{mk'i}$ does not collide with other devices in i-th cell, we can receive it. We adopt the maximum-ratio-combing (MRC) receiver here and process the data signal, which is given by

$$\begin{aligned}e_{mk'i} &= \hat{\mathbf{g}}_{imk'i}^H\mathbf{r}_i \\ &= \sqrt{P_{mk'i}}\hat{\mathbf{g}}_{imk'i}^H\mathbf{g}_{imk'i}x_{mk'i} + \sum_{n=1,n\neq m}^{N_k}\sqrt{P_{nk'i}}\hat{\mathbf{g}}_{imk'i}^H\mathbf{g}_{ink'i}x_{nk'i}\gamma_{nk'i} + \hat{\mathbf{g}}_{imk'i}^H\mathbf{o}_i \\ &+ \sum_{k=1,k\neq k'}^{K}\sum_{n=1}^{N_k}\sqrt{P_{nki}}\hat{\mathbf{g}}_{imk'i}^H\mathbf{g}_{inki}x_{nki}\gamma_{nki} + \sum_{l=1,l\neq i}^{L}\sum_{k=1}^{K}\sum_{n=1}^{N_k}\sqrt{P_{nkl}}\hat{\mathbf{g}}_{imk'i}^H\mathbf{g}_{inkl}x_{nkl}\gamma_{nkl}.\end{aligned} \tag{7}$$

Further, (7) can be represented as (8)

$$\begin{aligned}e_{mk'i} &= \sqrt{P_{mk'i}}\mathbb{E}_{\mathrm{h}}\left\{\hat{\mathbf{g}}_{imk'i}^H\mathbf{g}_{imk'i}\right\}x_{mk'i} + \sum_{n=1,n\neq m}^{N_k}\sqrt{P_{nk'i}}\hat{\mathbf{g}}_{imk'i}^H\mathbf{g}_{ink'i}x_{nk'i}\gamma_{nk'i} \\ &+ \sqrt{P_{mk'i}}\left[\hat{\mathbf{g}}_{imk'i}^H\mathbf{g}_{imk'i} - \mathbb{E}_{\mathrm{h}}\left\{\hat{\mathbf{g}}_{imk'i}^H\mathbf{g}_{imk'i}\right\}\right]x_{mk'i} + \hat{\mathbf{g}}_{imk'i}^H\mathbf{o}_i \\ &+ \sum_{k=1,k\neq k'}^{K}\sum_{n=1}^{N_k}\sqrt{P_{nki}}\hat{\mathbf{g}}_{imk'i}^H\mathbf{g}_{inki}x_{nki}\gamma_{nki} + \sum_{l=1,l\neq i}^{L}\sum_{k=1}^{K}\sum_{n=1}^{N_k}\sqrt{P_{nkl}}\hat{\mathbf{g}}_{imk'i}^H\mathbf{g}_{inkl}x_{nkl}\gamma_{nkl},\end{aligned} \tag{8}$$

where $\mathbb{E}_{\mathrm{h}}\{\bullet\}$ is the average of the small-scale fading. We further assume that the channel is ergodic so that an ergodic achievable uplink rate $R_{mk'i}$ of $\mathsf{U}_{mk'i}$ is given b

$$R_{mk'i} = \log_2\left(1 + \frac{\sqrt{P_{mk'i}}\left|\mathbb{E}_{\mathrm{h}}\left\{\hat{\mathbf{g}}_{imk'i}^H\mathbf{g}_{imk'i}\right\}\right|^2}{\mathcal{F}_{mk'i}}\right), \tag{9}$$

where $\mathcal{F}_{mk'i}$ is represented by

$$\begin{aligned}\mathcal{F}_{mk'i} &= \sqrt{P_{mk'i}}\mathbf{Var}\left\{\hat{\mathbf{g}}_{imk'i}^H\mathbf{g}_{imk'i}\right\} + \sum_{n=1,n\neq m}^{N_k}\sqrt{P_{nk'i}}\mathbb{E}_{\mathrm{h}}\left\{\left|\hat{\mathbf{g}}_{imk'i}^H\mathbf{g}_{ink'i}\right|^2\right\}\gamma_{nk'i} \\ &+ \sum_{k=1,k\neq k'}^{K}\sum_{n=1}^{N_k}\sqrt{P_{nki}}\mathbb{E}_{\mathrm{h}}\left\{\left|\hat{\mathbf{g}}_{imk'i}^H\mathbf{g}_{inki}\right|^2\right\}\gamma_{nki} + \mathbb{E}_{\mathrm{h}}\left\{\left\|\hat{\mathbf{g}}_{imk'i}^H\right\|^2\right\} \\ &+ \sum_{l=1,l\neq i}^{L}\sum_{k=1}^{K}\sum_{n=1}^{N_k}\sqrt{P_{nkl}}\mathbb{E}_{\mathrm{h}}\left\{\left|\hat{\mathbf{g}}_{imk'i}^H\mathbf{g}_{inkl}\right|^2\right\}\gamma_{nkl}\end{aligned} \tag{10}$$

The channel estimation is obtained when U_{nkl} does not collide with other devices in the cell. Let $\rho_{nkl} \in \{0,1\}$, where $\rho_{nkl} = 1$ denotes that U_{nkl} is an intra-cell non-colliding device and $\rho_{nkl} = 0$ that it is not an intra-cell non-colliding device. Then, average spectral efficiency of the k-th type of device in the i-th cell is given by

$$S_{ki} = \left(1 - \frac{\tau}{T}\right)\mathbb{E}\left\{\sum_{n=1}^{N_k}R_{nki}\rho_{nki}\right\}. \tag{11}$$

Since R_{nki} and ρ_{nki} are independent, (11) can be represented as

$$S_{ki}=\left(1-\frac{\tau}{T}\right)\sum_{n=1}^{N_k}\mathbb{E}\{R_{nki}\}\mathbb{E}\{\rho_{nki}\}=\left(1-\frac{\tau}{T}\right)\mathcal{R}_{ki}N_{\text{non},k}, \tag{12}$$

where $\mathcal{R}_{ki}=\mathbb{E}\{R_{nki}\}$ is got by averaging the parameters such as large-scale fading, pilot selection and device activation of R_{nki}, which eliminates the difference among devices in the same cell and the corresponding subscript is omitted, and $N_{\text{non},k}=\sum_{n=1}^{N_k}\mathbb{E}\{\rho_{nki}\}$ indicates the average number of intra-cell non-colliding devices of the k-th type device per cell. Hence, the average spectral efficiency per cell is further written as

$$S_i=\sum_{k=1}^{K}S_{ki}. \tag{13}$$

Next, we give the expressions for the average number of intra-cell non-colliding devices of the k-th type device per cell.

Lemma 1. The distributions of the indicator γ_{nkl} and $\delta_{nkl}^{(mk'i)}$ are

$$\mathbb{P}[\gamma_{nkl}=1]=p_{\text{b},k},\ \mathbb{P}\left[\delta_{nkl}^{(mk'i)}=1\middle|l\in\mathcal{C}_i\right]=\alpha p_{\text{b},k}/\tau. \tag{14}$$

The average number of intra-cell non-colliding devices of the k-th type device per cell can be written as

$$N_{\text{non},k}=\sum_{n=1}^{N_k}n\binom{N_K}{n}p_{\text{b},k}^{n}\left(1-p_{\text{b},k}\right)^{N_k-n}\left(1-\frac{\alpha}{\tau}\right)^{\left(\sum_{k=1}^{K}p_{\text{b},k}N_k-1\right)}. \tag{15}$$

Proof. See Appendix A:

In the above results, we can see that $N_{\text{non},k}$ is related to τ and the parameters of devices, and it is not only affected by its own activation probability and number, but also by the activation probability and number of other types in the cell. When the system model reduce to a single cell with one type of device, (15) becomes $N_{\text{no-colli}}=N_{\text{tatal}}p_b(1-\frac{1}{\tau})^{N_{\text{tatal}}p_b-1}$, where N_{total} is the total number of devices, and p_{b} is the backoff probability. We can find that $N_{\text{no-colli}}$ is the same as (1) in [18].

We use the power control technique to compensate for the large-scale fading of devices in each cell. The power control factor is given by $\lambda=P_{nkl}\beta_{inkl}$ (for any n, k, and l). Then, with it we can substitute $N_{\text{non},k}$ from (15) into (12) to get S_i.

Theorem 1. The approximation of the average spectral efficiency of the i-th cell is given by

$$S_i=\sum_{k=1}^{K}S_{ki}, \tag{16}$$

where S_{ki} is as follows

$$S_{ki}\approx\left(1-\frac{\tau}{T}\right)N_{\text{non},k}\log_2\left(1+\frac{\tau M\lambda^2}{\mathcal{Q}}\right), \tag{17}$$

in which $\mathcal{Q}$ is given by (18). In (18), $\mathcal{P}$ denotes the average transmitted power of all devices,

$$\begin{aligned}\mathcal{Q} &= (\tau\lambda+1)\lambda\left[p_{\mathrm{b},k'}\left(N_{k'}-1\right)+\sum_{k=1,k\neq k'}^{K}p_{\mathrm{b},k}N_k\right]+(\tau\lambda+1)(\lambda+1)\\ &+\mathcal{P}^2\alpha\left(\sum_{k=1}^{K}p_{\mathrm{b},k}N_k\right)\left[1+p_{\mathrm{b},k'}\left(N_{k'}-1\right)+\sum_{k=1,k\neq k'}^{K}p_{\mathrm{b},k}N_k\right]\sum_{l\in\mathcal{C}_i\setminus i}\varepsilon_{ikl}^2\\ &+\mathcal{P}^2\alpha\left(\sum_{k=1}^{K}p_{\mathrm{b},k}N_k\right)^2\sum_{l_1=1,l_1\neq i}^{L}\sum_{l_2\in\mathcal{C}_i\setminus i,l_2\neq l_1}\varepsilon_{ikl_1}\varepsilon_{ikl_2}+\mathcal{P}^2M\alpha\left(\sum_{k=1}^{K}p_{\mathrm{b},k}N_k\right)\sum_{l\in\mathcal{C}_i\setminus i}\mu_{ikl}\\ &+\mathcal{P}\left(\sum_{k=1}^{K}p_{\mathrm{b},k}N_k\right)\left\{\alpha\tau+\alpha+1+\tau\lambda+\alpha\lambda\left[p_{\mathrm{b},k'}\left(N_{k'}-1\right)+\sum_{k=1,k\neq k'}^{K}p_{\mathrm{b},k}N_k\right]\right\}\sum_{l\in\mathcal{C}_i\setminus i}\varepsilon_{ikl}.\end{aligned} \tag{18}$$

while $\varepsilon_{ikl}=\mathbb{E}\{\beta_{inkl}\}$ and $\mu_{ikl}=\mathbb{E}\left\{\beta_{inkl}^2\right\}$ represent the average and average square of large-scale fading from a device of the k-th type in the l-th cell to the i-th BS.

Proof. See Appendix B:

The above results are averaged for all randomness, such as device activation, and pilot selection. That is, strong versatility, suitable for most networks. Obviously, S_i is not a monotone function of $p_{\mathrm{b},k}$, so we need to find the optimal value for $p_{\mathrm{b},k}$. Next, we look for the optimal $p_{\mathrm{b},k}$ to maximize (16).

3.3 Optimal backoff parameters

In this section, we aim to find the optimal $p_{\mathrm{b},k}$ for each type of device that maximize S_i. That is, to solve the following optimization problem.

$$\begin{aligned}(P1)\quad &\max_{p_{\mathrm{b},1}^*,\ldots,p_{\mathrm{b},K}^*} \quad S_i\\ &s.t. \quad 0<p_{\mathrm{b},k}\leq 1,\forall k\\ &\qquad 0<\mathcal{D}_k\leq\mathcal{D}_k^{\mathrm{u}},\forall k.\end{aligned} \tag{19}$$

Because of the backoff mechanism, it takes time for each user to access, and the time required for user access is called access delay. We use $\mathcal{D}_k$ to denote the delay for the k-th type of device. Considering that devices in IoT usually short time requirements, we set delay constraints for the k-th type of devices as $\mathcal{D}_k^{\mathrm{u}}$, i.e., the maximum permissible delay for the k-th type of devices. Note that the unit of delay constraints is time slot and will not be specified for simplication. From an average point of view, $\mathcal{D}_k=1/p_{\mathrm{b},k}$. Therefore, $(P1)$ can be simplified into $(P2)$.

$$\begin{aligned}(P2)\quad &\max_{p_{\mathrm{b},1}^*,\ldots,p_{\mathrm{b},K}^*} \quad S_i\\ &s.t. \quad \frac{1}{\mathcal{D}_k^{\mathrm{u}}}<p_{\mathrm{b},k}\leq 1,\forall k.\end{aligned} \tag{20}$$

For $(P2)$, we use gradient descent. $p_{\mathrm{b},k}$ is iterated continuously until S_i converges, and the specific algorithm details can be summarized in algorithm 1, as shown in **Table 2**.

We also analyze the complexity of algorithm 1. We can see that the complexity of algorithm 1 depends on the gradient of the backoff probability. The main overall complexity is

$O(tKN_k + tK + tK\vartheta + 2tK^2\vartheta + tK^2L\vartheta)$, where ϑ is the number of co-pilot cells in the i-th cell [25]. Therefore, we can see that the algorithm complexity mainly depends on the number of device types, the number of devices and the number of co-pilot cells.

Table 2. Optimization algorithm

Algorithm 1 Alternating Optimization Algorithm for (P2)

Initialization: $p_{\mathrm{b},k}^0 = p_{\mathrm{b},k}^{ran}$, the search step $\nu_1 = 0.1$, $\nu_2 = 1$, the error $\Xi = 10^{-6}$, and the iterate number $t = 0$

1: **repeat**
2: **for** $k = 0,1,\ldots,K$ **do**
3: **for** $t = 0,1,\ldots$ **do**
4: calculate the gradient vector Q^t
5: calculate $p_{\mathrm{b},k}^{t+1} = p_{\mathrm{b},k}^t + \nu_1 Q^t$
6: determine whether the $p_{\mathrm{b},k}^{t+1}$ dissatisfies (20), if it is, let $p_{\mathrm{b},k}^{t+1} = p_{\mathrm{b},k}^t - \nu_2 Q^t$, goon 7
7: calculate the average spectral efficiency $S_i\left(p_{\mathrm{b},k}^{t+1}\right)$
8: update $t = t+1$. Until $\left|S_i\left(p_{\mathrm{b},k}^{t+1}\right) - S_i\left(p_{\mathrm{b},k}^t\right)\right| < \Xi$, $p_{\mathrm{b},k}^{opt} = p_{\mathrm{b},k}^{t+1}$
9: **end for**
10: **end for**

Output: $\mathbf{P} = \left[p_{\mathrm{b},1}^{opt},\ldots,p_{\mathrm{b},K}^{opt}\right]^T$

4. Numerical Results

In this section, we consider two types of devices exists in the network, denoted as device 1 and 2, respectively. Devices are randomly and uniformly distributed in a cell with a radius of $r_c = 1000$ meters, and there is an area with a radius of $r_h = 100$ meters in the middle where no devices are distributed. The large-scale fading model is expressed as $\beta_{inkl} = z_{inkl} / (r_{inkl}/r_h)^{\upsilon}$, where z_{inkl} is a log-normal random variable with standard deviation σ, υ is the path loss exponent, and r_{inkl} is the distance between U_{nkl} and the i-th BS. We assume that $\sigma = 8$ dB and $\upsilon = 3.8$. ε_{ikl} and μ_{ikl} are got by averaging over 1000 realizations of devices spatial distributions in each cell. We assume that the data is transmitted using an OFDM system and $T = 196$ symbols. We set $\lambda = 0.1$ and $\alpha = 3$.

4.1 Performance Validation

In **Fig. 2**, we compare the simulated spectral efficiency in (11) and the analytic approximation in (16). Clearly, in all cases, no matter with a small or large τ, the analytical value and the simulation value are very tight, which indicates the accuracy and rigor of our analysis results. Given the tightness, we use the analysis results of (16) for the following investigations.

4.2 Performance Analysis

In **Fig. 3**, we study the relationship between the backoff probability of devices and the average

spectral efficiency. We use $p_{\mathrm{b},1}$ and $p_{\mathrm{b},2}$ to represent the backoff probability of device 1 and device 2, respectively. Firstly, we find that with the increase of $p_{\mathrm{b},1}$, the average spectral efficiency S_i keeps growing until it reaches a critical point, and gradually decrease. This is because when backoff probability is small, there are few active devices connected to the system. Therefore, pilots are sufficient for devices and S_i will increase with growth of active devices, i.e., the growth of backoff probability. However, when backoff probability increases to a critical point, the number of active devices exceeds the number of pilots. Therefore, the pilot collision is aggravated when active devices grows and S_i begin to reduce. Given that, we find that there exists an optimal backoff probability that maximizes S_i. Secondly, it can be seen from **Fig. 3** that when τ is fixed, the optimal backoff probability decreases with the increment of the device number. Conversely, when the number of devices is fixed, the optimal backoff probability decreases with the decrement of τ. Next, we discuss the variation of the optimal backoff probability with respect to devices number and delay constraints.

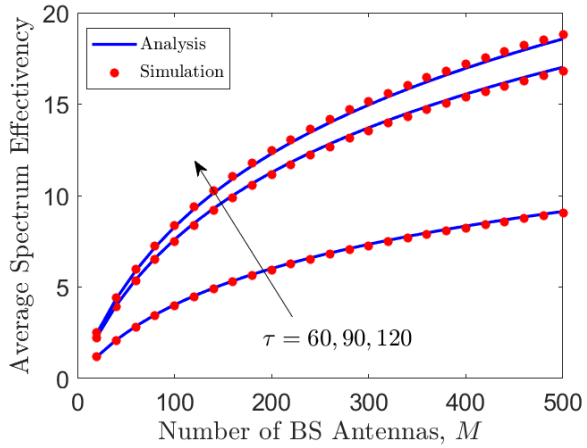

Fig. 2. Average spectral efficiency per cell vs. BS antenna number, where $p_{\mathrm{b},1} = p_{\mathrm{b},2} = 0.5$.

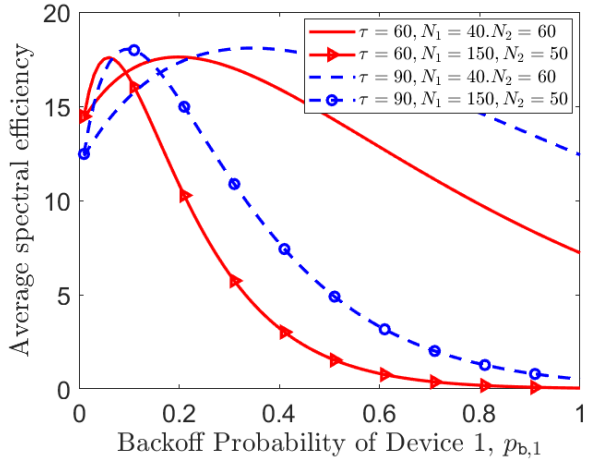

Fig. 3. Average spectral efficiency per cell vs. backoff probability, where $M = 200$, and $p_{\mathrm{b},1} = p_{\mathrm{b},2}$.

Fig. 4 shows the optimal backoff probability with and without delay constraints, where the number of device 2 is fixed ($N_2 = 140$). **Fig. 4. (a)** is the case without delay constraints, and it can be seen that when $N_1 < N_2$, $p_{\mathrm{b},1} > p_{\mathrm{b},2}$; and when $N_1 > N_2$, $p_{\mathrm{b},1} < p_{\mathrm{b},2}$. This indicates that devices with larger quantity should have more backoff time. When the total number of devices in a cell is large, the type of devices that have larger quantity backoff altogether, that is, the access opportunity should be completely transferred to devices with smaller quantity. **Fig. 4. (b)** is the case with delay constraints. It can be seen that due to delay constraints, devices with larger quantity cannot completely backoff, and their optimal backoff probability is the lower bound determined by delay constraints. Moreover, when there is a large number of devices in the cell, the lower bound is taken for both devices with larger quantity and devices with smaller quantity.

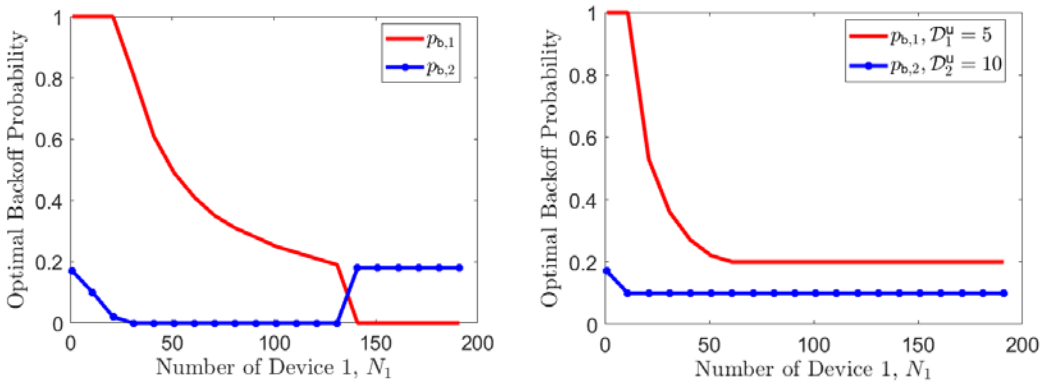

(a) Without Delay Constraints (b) With Delay Constraints

Fig. 4. Optimal backoff probability vs. number of device 1, where $N_2 = 140$, and $M = 200$.

Now, we discuss the influence of delay constraints on the optimal backoff probability. **Fig. 5** shows the change of optimal backoff probability of two devices with different numbers when $\mathcal{D}_2^{\mathrm{u}}$ is fixed ($\mathcal{D}_2^{\mathrm{u}} = 10$). It can be seen that with the increment of $\mathcal{D}_1^{\mathrm{u}}$, the optimal $p_{\mathrm{b},1}$ decreases and is always at the lower limit of its feasible region due to delay constraints, while the optimal $p_{\mathrm{b},2}$ first lies a the lower bound and then grow up to exceed the $p_{\mathrm{b},1}$ when $\mathcal{D}_1^{\mathrm{u}}$ increases. This indicates that a larger number of devices should be allocated more backoff time when delay constraints are relatively loose. However, as delay constraints become stricter, the required backoff time of this type of devices reduces, and may even be less than devices with smaller quantity in the case with extremely strict delay constraints.

Fig. 6 shows how the optimal backoff probability of the two types of devices varies with respect to delay constraints where $\mathcal{D}_1^{\mathrm{u}} = \mathcal{D}_2^{\mathrm{u}}$. We can see that when the number of device 1 remains unchanged and the number of device 2 increases from 60 to 130 , the optimal $p_{\mathrm{b},1}$ and optimal $p_{\mathrm{b},2}$ are the same as the lower limit of the feasible domain under strict delay constraints, which confirms the conclusion of **Fig. 5**. Moreover, we compare the optimal backoff probability under $\tau = 90$ and $\tau = 120$, and find that in the case with large τ , the optimal backoff probability has a stronger tolerance to delay constraints, and the system can accommodate more devices to access. When τ is small, the optimal backoff probability take the lower limit of the feasible region more often than that with large τ , which indicates that

the effect of delay constraints works more obviously when the pilot length is short.

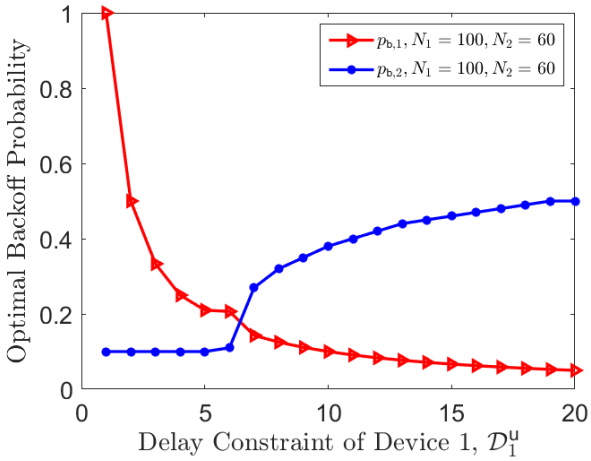

Fig. 5. Optimal backoff probability vs. delay constraints of device 1, where $\mathcal{D}_2^{\mathrm{u}} = 10$, and $M = 200$.

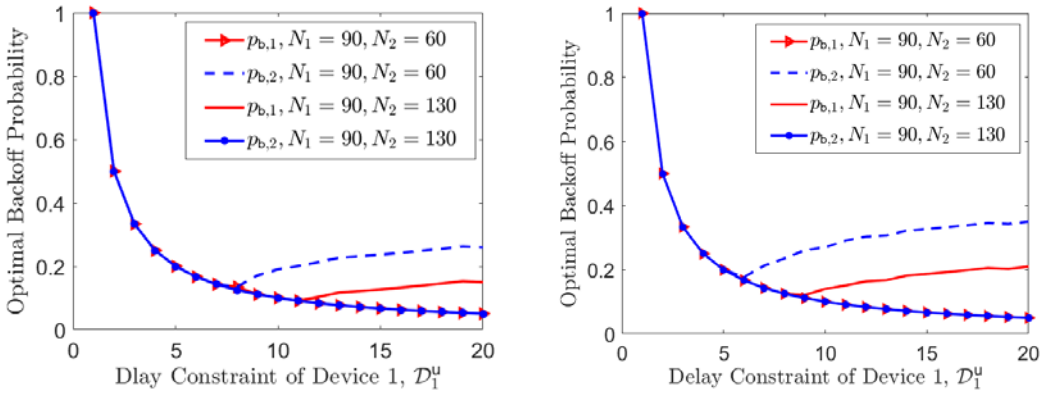

(a) $\tau = 90$ (b) $\tau = 120$

Fig. 6. Optimal backoff probability vs. delay constraints of device 1, where $\mathcal{D}_1^{\mathrm{u}} = \mathcal{D}_2^{\mathrm{u}}$, and $M = 200$.

In **Fig. 7**, we compare the average spectral efficiency S_i with full access, i.e., $p_{\mathrm{b},k} = 1$, with the optimal backoff mechanism we proposed. It can be seen that when N_1 increases gradually, S_i increases first and then tends to be stable with optimal $p_{\mathrm{b},k}$, but S_i with $p_{\mathrm{b},k} = 1$ increases first and then decreases. It can be seen that the system with optimal backoff mechanism is obviously better than the system without backoff mechanism. We also find that with the increment of the number of devices, the advantage of the optimal backoff mechanism becomes more obvious, i.e., the gain of S_i also increases. Therefore, in large user scenarios, which is a typical scenario in IoT, it is necessary to adopt the optimal backoff mechanism we proposed.

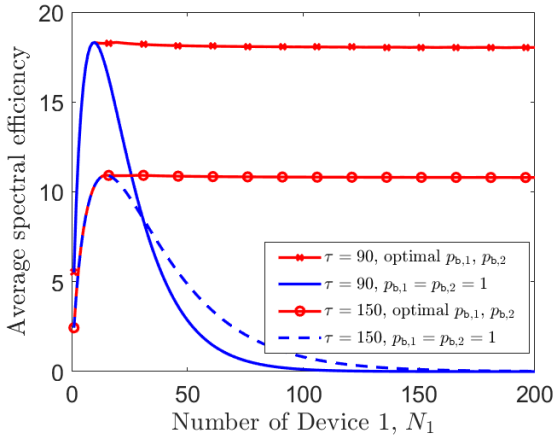

Fig. 7. Average spectral efficiency per cell vs. number of device 1, where $N_1 = N_2$, and $M = 200$.

5. Conclusion

This paper has investigated the GFRA in multicell massive MIMO systems with mixed-type devices with delay constraints. The analytic approximation of the average spectral efficiency is derived by using indicators which captured devices' behaviors uncertainty and verified by simulation. we obtain the optimal backoff parameter for each type of devices under their delay constraints. It is found that the optimal backoff parameters are closely related to the devices number and delay constraints. In general, devices that have larger quantity should have more backoff time before they are allowed to access. However, as delay constraints become stricter, the required backoff time of devices reduces gradually, and the device with larger quantity may have less backoff time than that with smaller quantity when its delay constraint is extremely strict. Moreover, when the pilot length is short, the effect of delay constraints mentioned above works more obviously. In conclusion, the system with backoff mechanism is more practical and has better performance. Especially in the scenario of IoT, it is necessary to adopt the optimal backoff mechanism proposed by us.

Appendix

Appendix A

We assume that the U_{nkl} is active, and $A_{\text{non},k}$ indicates the number of other k-th devices in the l-th cell that non-collide with U_{nkl}. We use $N_{\text{non},k}$ to represent the average number of intra-cell non-colliding devices of the k-th type device per cell. According to the backoff probability of each type of device, we can get that the average number of active devices of the k-th type is $p_{\text{b},k}N_k$. Therefore, the probability that each device does not collide with other devices in the same cell is

$$p_k = \left(1 - \frac{\alpha}{\tau}\right)^{\left(\sum_{k=1}^{K} p_{\text{b},k}N_k - 1\right)}. \tag{21}$$

Then, based on (14) and (21), using the binomial theorem, $N_{\text{non},k}$ can be written as

$$N_{\text{non},k} = \mathbb{E}\left\{A_{\text{non},k}\right\} = \sum_{n=1}^{N_k} n \binom{N_k}{n} p_{\text{b},k}^{n} \left(1 - p_{\text{b},k}\right)^{N_k - n} p_k. \tag{22}$$

By substituting (21) into (22), we can get the final result.

Appendix B

From (4), and with some basic math, we know that

$$\mathbb{E}_{\text{h}}\left\{\hat{\mathbf{g}}_{imk'i}^{H}\mathbf{g}_{imk'i}\right\} = M\beta_{imk'i}. \tag{23}$$

Let $\zeta_{imk'i} = \beta_{imk'i} + \sum_{l\in\mathcal{C}_i\setminus i}\sum_{k=1}^{K}\sum_{n=1}^{N_k}\frac{P_{nkl}}{P_{imk'i}}\beta_{inkl}\delta_{nkl}^{(imk'i)} + \frac{1}{\sqrt{\tau P_{imk'i}}}$, then

$$\mathbb{E}_{\text{h}}\left\{\left\|\hat{\mathbf{g}}_{imk'i}^{H}\right\|^2\right\} = M\zeta_{imk'i}, \tag{24}$$

$$\mathbb{E}_{\text{h}}\left\{\chi_1\right\} = \begin{cases} M^2\beta_{imk'i}^2 + M\beta_{imk'i}\zeta_{imk'i}, & \left(m,k' \neq n,k\right) \\ M\beta_{inki}\zeta_{imk'i}, & \left(m,k' = n,k\right) \end{cases}, \tag{25}$$

where $\chi_1 = \left|\hat{\mathbf{g}}_{imk'i}^{H}\mathbf{g}_{inki}\right|^2$.

$$\mathbb{E}_{\text{h}}\left\{\chi_2\right\} = \begin{cases} \frac{P_{nkl}}{P_{mk'i}}M^2\beta_{inkl}^2 + M\beta_{inkl}\zeta_{imk'i}, & \delta_{nkl}^{(mk'i)} = 1 \\ M\beta_{inkl}\zeta_{imk'i}, & \delta_{nkl}^{(mk'i)} = 0 \end{cases}, \tag{26}$$

where $\chi_2 = \left|\hat{\mathbf{g}}_{imk'i}^{H}\mathbf{g}_{inkl}\right|^2$.

Substitute the above conclusion into (9), then

$$R_{mk'i} = \log_2\left(1 + \frac{\tau P_{mk'i}^2 M\beta_{imk'i}^2}{\boldsymbol{\psi}_1}\right), \tag{27}$$

where

$$\begin{aligned} \boldsymbol{\psi}_1 = &\left(\tau P_{mk'i}\beta_{imk'i} + 1\right)\Omega_1 + \left(\tau P_{mk'i}\beta_{imk'i} + \tau\right)\Omega_2 + \tau\Omega_1\Omega_2 \\ &+ \tau M P_{nkl}\Omega_3 + \tau P_{mk'i}^2\beta_{imk'i}^2 + P_{mk'i}\beta_{imk'i} + \tau P_{mk'i}\beta_{imk'i} + 1, \end{aligned} \tag{28}$$

and

$$\begin{aligned} \Omega_1 &= \sum_{n=1,n\neq m}^{N_k} P_{nk'i}\beta_{ink'i}\gamma_{nk'i} + \sum_{k=1,k\neq k'}^{K}\sum_{n=1}^{N_k} P_{nki}\beta_{inki}\gamma_{nki} + \sum_{l=1,l\neq i}^{L}\sum_{k=1}^{K}\sum_{n=1}^{N_k} P_{nkl}\beta_{inkl}\gamma_{nkl}, \\ \Omega_2 &= \sum_{l\in\mathcal{C}_i\setminus i}\sum_{k=1}^{K}\sum_{n=1}^{N_k} P_{nkl}\beta_{inkl}\delta_{nkl}^{(mk'i)}, \\ \Omega_3 &= \sum_{l\in\mathcal{C}_i\setminus i}\sum_{k=1}^{K}\sum_{n=1}^{N_k} P_{nkl}\beta_{inkl}^2\delta_{nkl}^{(mk'i)}. \end{aligned} \tag{29}$$

For the power control factor, let $\varepsilon_{ikl} = \mathbb{E}\left\{\beta_{inkl}\right\}$, $\mu_{ikl} = \mathbb{E}\left\{\beta_{inkl}^2\right\}$, and the average transmitting power of all devices is denoted by $\mathcal{P}$ and then substituted into (26). Therefore, using Jensen's inequality, (26) can be written as

$$\mathbb{E}\left\{R_{mk'i}\right\} \approx \mathbb{E}\left\{\log_2\left(1+\frac{\tau M \lambda^2}{\psi_2}\right)\right\} \geq \log_2\left(1+\frac{\tau M \lambda^2}{\mathbb{E}\left\{\psi_2\right\}}\right), \tag{30}$$

where

$$\begin{aligned}\psi_2 = &(\tau\lambda+1)\bar{\Omega}_1 + (\tau\lambda+\tau)\bar{\Omega}_2 + \tau\bar{\Omega}_1\bar{\Omega}_2 \\ &+\tau M \mathcal{P}\bar{\Omega}_3 + \tau\lambda^2 + \lambda + \tau\lambda + 1,\end{aligned} \tag{31}$$

and

$$\begin{aligned}\bar{\Omega}_1 &= \sum_{n=1,n\neq m}^{N_k} \lambda\gamma_{nk'i} + \sum_{k=1,k\neq k'}^{K}\sum_{n=1}^{N_k}\lambda\gamma_{nki} + \sum_{l=1,l\neq i}^{L}\sum_{k=1}^{K}\sum_{n=1}^{N_k}\mathcal{P}\varepsilon_{ikl}\gamma_{nkl}, \\ \bar{\Omega}_2 &= \sum_{l\in\mathcal{C}_i'\setminus i}\sum_{k=1}^{K}\sum_{n=1}^{N_k}\mathcal{P}\varepsilon_{inkl}\delta_{nkl}^{(mk'i)}, \\ \bar{\Omega}_3 &= \sum_{l\in\mathcal{C}_i'\setminus i}\sum_{k=1}^{K}\sum_{n=1}^{N_k}\mathcal{P}\mu_{nkl}\delta_{nkl}^{(mk'i)}.\end{aligned} \tag{32}$$

Then, from Lemma 1, we can get that

$$\begin{aligned}\mathbb{E}\left\{\bar{\Omega}_1\right\} &= \lambda p_{\mathrm{b},k}\left(N_{k'}-1\right) + \lambda\left(\sum_{k=1,k\neq k'}^{K} p_{\mathrm{b},k}N_k\right) + \mathcal{P}\left(\sum_{k=1}^{K} p_{\mathrm{b},k}N_k\right)\sum_{l=1,l\neq i}^{L}\varepsilon_{ikl}, \\ \mathbb{E}\left\{\bar{\Omega}_2\right\} &= \mathcal{P}\frac{\alpha}{\tau}\left(\sum_{k=1}^{K} p_{\mathrm{b},k}N_k\right)\sum_{l\in\mathcal{C}_i'\setminus i}\varepsilon_{ikl}, \\ \mathbb{E}\left\{\bar{\Omega}_3\right\} &= \mathcal{P}\frac{\alpha}{\tau}\left(\sum_{k=1}^{K} p_{\mathrm{b},k}N_k\right)\sum_{l\in\mathcal{C}_i'\setminus i}\mu_{ikl}.\end{aligned} \tag{33}$$

If $(n_1,k_1,l_1)=(n_2,k_2,l_2)$, $\mathbb{E}\left\{\gamma_{n_1,k_1,l_1}\delta_{n_2,k_2,l_2}^{(mk'i)}\right\} = p_{\mathrm{b},k_1}\frac{\alpha}{\tau}$; and if $(n_1,k_1,l_1)\neq(n_2,k_2,l_2)$, $\mathbb{E}\left\{\gamma_{n_1,k_1,l_1}\delta_{n_2,k_2,l_2}^{(mk'i)}\right\} = p_{\mathrm{b},k_1}p_{\mathrm{b},k_2}\frac{\alpha}{\tau}$. Therefore, we can get

$$\begin{aligned}\mathbb{E}\left\{\bar{\Omega}_1\bar{\Omega}_2\right\} = &\lambda\mathcal{P}\frac{\alpha}{\tau}\left(\sum_{k=1}^{K} p_{\mathrm{b},k}N_k\right)\left[p_{\mathrm{b},k'}\left(N_{k'}-1\right) + \sum_{k=1,k\neq k'}^{K} p_{\mathrm{b},k}N_k\right]\sum_{l\in\mathcal{C}_i'\setminus i}\varepsilon_{ikl} \\ &+\mathcal{P}^2\frac{\alpha}{\tau}\left(\sum_{k=1}^{K} p_{\mathrm{b},k}N_k\right)\left[1+p_{\mathrm{b},k'}\left(N_{k'}-1\right) + \sum_{k=1,k\neq k'}^{K} p_{\mathrm{b},k}N_k\right]\sum_{l\in\mathcal{C}_i'\setminus i}\varepsilon_{ikl}^2 \\ &+\mathcal{P}^2\frac{\alpha}{\tau}\left(\sum_{k=1}^{K} p_{\mathrm{b},k}N_k\right)^2\sum_{l_1=1,l_1\neq i}^{L}\sum_{l_2\in\mathcal{C}_i'\setminus i,l_2\neq l_1}\varepsilon_{ikl_1}\varepsilon_{ikl_2}.\end{aligned} \tag{34}$$

Then, by substituting (33) and (34) into (30), we can get the final result.

Acknowledgement

This work was supported in part by the Graduate Research and Innovation Projects of Jiangsu Province under SJCX21_0263. The work of Qi Zhang was supported in part by the National Natural Science Foundation of China under Grant 62171231 and 61801244, in part by the National Key Research & Development Program of China under Grant No. 2020YFB1807202.

References

[1] J. Li, M. Wen and T. Zhang, "Group-Based Authentication and Key Agreement With Dynamic Policy Updating for MTC in LTE-A Networks," *IEEE Internet Things J.*, vol. 3, no. 3, pp. 408–417, Jun. 2016. Article (CrossRef Link)

[2] X. Liu, T. Huang, N. Shlezinger, Y. Liu, J. Zhou and Y. C. Eldar, "Joint transmit beamforming for multiuser MIMO communications and MIMO radar," *IEEE Trans. Signal Process.*, vol. 68, pp. 3929-3944, 2020. Article (CrossRef Link)

[3] H. Q. Ngo, E. G. Larsson, and T. L. Marzetta, "Energy and spectral efficiency of very large multiuser MIMO systems," *IEEE Trans. Commun.*, vol. 61, no. 4, pp. 1436–1449, Apr. 2013. Article (CrossRef Link)

[4] M. Y. Ali, T. Hossain, and M. M. Mowla, "A trade-off between energy and spectral efficiency in massive MIMO 5G system," in *Proc. of ICECTE*, Rajshahi, Bangladesh, pp. 209–212, 2019. Article (CrossRef Link)

[5] O. Mahmoud and A. El-Mahdy, "Performance evaluation of noncoherent DPSK signal detection algorithms in massive MIMO systems," in *Proc. of Conf. TELE*, Leiria, Portugal, pp. 1–5, 2021. Article (CrossRef Link)

[6] T. Wang, Y. Wang, C. Wang, Z. Yang and J. Cheng, "Group-based random access and data transmission scheme for massive MTC networks," *IEEE Trans. Commun.*, vol. 69, no. 12, pp. 8287-8303, Dec. 2021. Article (CrossRef Link)

[7] J. Choi, "Fast retrial for low-latency connectivity in MTC with two different types of devices," *IEEE Wireless Commun. Lett.*, vol. 9, no. 10, pp. 1786-1789, Oct. 2020. Article (CrossRef Link)

[8] Z. Chen, F. Sohrabi, and W. Yu, "Multi-cell sparse activity detection for massive random access: Massive MIMO versus cooperative MIMO," *IEEE Trans. Wireless Commun.*, vol. 18, no. 8, pp. 4060–4074, Aug. 2019. Article (CrossRef Link)

[9] X. Fang, M. Zhao, S. Zhang, W. Zhou, and J. Zhu, "Grouping-based grant-free random access based on statistical distribution of user rates," in *Proc. of ICC*, Shanghai, China, pp. 1–6, 2019. Article (CrossRef Link)

[10] H. Han, L. Fang, W. Lu, K. Chi, W. Zhai and J. Zhao, "A novel grant-based pilot access scheme for crowded massive MIMO systems," *IEEE Trans. Veh. Technol.*, vol. 70, no. 10, pp. 11111-11115, Oct. 2021. Article (CrossRef Link)

[11] O. S. Nishimura, J. C. Marinello and T. Abrão, "A grant-based random access protocol in extra-large massive MIMO system," *IEEE Wireless Commun. Lett*, vol. 24, no. 11, pp. 2478-2482, Nov. 2020. Article (CrossRef Link)

[12] A. T. Abebe and C. G. Kang, "Multi-sequence spreading random access (MSRA) for compressive sensing-based grant-free communication," *IEEE Trans. Commun.*, vol. 69, no. 11, pp. 7531–7543, Nov. 2021. Article (CrossRef Link)

[13] Technical specification group services and system aspects, 2-step RACH for NR, document 3GPP TR 21.916 (V16.2.0), 3GPP, June. 2022. [Online]. Available: https://www.3gpp.org/ftp/Specs/archive/21_series/21.916

[14] J. Ding, M. Feng, M. Nemati, and J. Choi, "Performance analysis of massive MIMO assisted semi-grant-free random access," in *Proc. of CCNC*, Las Vegas, NV, USA, pp. 1–7, 2021. Article (CrossRef Link)

[15] Y. Liu, M. Zhao, L. Xiao and S. Zhou, "Pilot domain NOMA for grant-free massive random access in massive MIMO marine communication system," *China Commun.*, vol. 17, no. 6, pp. 131-144, June 2020. Article (CrossRef Link)

[16] Z. Zhang, Y. Li, C. Huang, Q. Guo, L. Liu, C. Yuen, and Y. L. Guan, "User activity detection and channel estimation for grant-free random access in LEO satellite-enabled internet of things," *IEEE Internet Things J.*, vol. 7, no. 9, pp. 8811–8825, Sept. 2020. Article (CrossRef Link)

[17] J. Ding and J. Choi, "Preamble-data superposition random access in massive MIMO systems," *IEEE Wireless Commun. Lett.*, vol. 9, no. 6, pp. 906–910, June 2020. Article (CrossRef Link)

[18] H. Jiang, D. Qu, J. Ding, and T. Jiang, "Multiple preambles for high success rate of grant-free random access with massive MIMO," *IEEE Trans. Wireless Commun.*, vol. 18, no. 10, pp. 4779–4789, Oct. 2019. Article (CrossRef Link)
[19] J. Ding, D. Qu, and H. Jiang, "Optimal preamble length for spectral efficiency in grant-free RA with massive MIMO," in *Proc. of ICEIC*, Auckland, New Zealand, pp. 1–5, 2019. Article (CrossRef Link)
[20] H. Wang, X. Zhang, and S. Zhou, "Analysis of system capacity of grant-free access with massive MIMO," in *Proc. of ICCC Workshops*, Xiamen, China, pp. 410–415, 2021. Article (CrossRef Link)
[21] Z. Chen, F. Sohrabi, and W. Yu, "Multi-cell sparse activity detection for massive random access: Massive MIMO versus cooperative MIMO," *IEEE Trans. Wireless Commun.*, vol. 18, no. pp. 4060-4074, Aug. 2019. Article (CrossRef Link)
[22] Medium Access Control (MAC) protocol specification, backoff parameter values, document 3GPP TS 36.321 (V10.3.0), 3GPP, Sept. 2011. [Online]. Available: https://www.3gpp.org/ftp/Specs/archive/36_series/36.321
[23] P. Jiang, H. Wang and M. De Mari, "Optimal dynamic backoff for grant-free NOMA IoT networks: a mean field game approach," in *Proc. of ICCC*, Sanshui, Foshan, China, pp. 997-1002, 2022. Article (CrossRef Link)
[24] J. Ding, D. Qu, H. Jiang and T. Jiang, "Success probability of grant-free random access with massive MIMO," *IEEE Internet of Things Journal*, vol. 6, no. 1, pp. 506-516, Feb. 2019. Article (CrossRef Link)
[25] G. Lei, Y. Liu and X. Xiao, "Analysis of joint transmit and receive antenna selection in CPM MIMO systems" *KSII Transactions on Internet and Information Systems*, vol. 11, no. 3, pp. 1425-1440, Mar. 2017. Article (CrossRef Link)

Yingying Fang is currently pursuing the M.Sc. degree in communication engineering with the Nanjing University of Posts and Telecommunications. Her research interests include massive MIMO communication and random access.

Qi Zhang received the B.S. and Ph.D. degrees in electrical and information engineering from the Nanjing University of Posts and Telecommunications (NJUPT), Nanjing, China, in 2010 and 2015, respectively. She was a Postdoctoral Research Fellow with the Singapore University of Technology and Design, Singapore, from 2015 to 2017. She is currently with the faculty of the Jiangsu Key Laboratory of Wireless Communications, NJUPT. Her research interests include massive MIMO systems, space–time wireless communications, heterogeneous cellular networks, and Internet of Things.